Hydrological and Runoff Formation Processes Based on Isotope Tracing During Ablation Period in the Source Regions of Yangtze River

Zong-Jie Li[1*], Zong-Xing Li[2*], Ling-Ling Song[3], Juan Gui[2], Jian Xue[2], Bai Juan Zhang[1], Wen De Gao[1]

[1]College of Energy and Power Engineering, Lanzhou University of Technology, Lanzhou 730050, China

[2]Observation and Research Station of Eco-Hydrology and Environmental Protection by Stable Isotope Tracing in High and Cold Mountainous Areas /Key Laboratory of Ecohydrology of Inland River Basin/Gansu Qilian Mountains Ecology Research Center, Northwest Institute of Eco-Environment and Resources, Chinese Academy of Sciences, Lanzhou 730000, China

[3]College of Forestry, Gansu Agricultural University, Lanzhou, Gansu 730070, China

*Corresponding author: Tel: 86+18993033525, E-mail: lzjie314@163.com (Zong-Jie Li), lizxhhs@163.com (Zong-Xing Li).

Abstract: This study focused on the hydrological and runoff formation processes of river water by using stable isotope tracing in the source regions of the Yangtze river during different ablation episodes in 2016 and the ablation period from 2016 to 2018. The effects of altitude on stable isotope characteristics for the river in the glacier permafrost area were greater than for the mainstream and the permafrost area during the ablation period in 2016. There was a significant negative correlation (at the 0.01 level) between precipitation and $\delta^{18}O$, while a significant positive correlation was evident between precipitation and d-excess. More interestingly, significant negative correlations appeared between $\delta^{18}O$ and temperature, relative humidity, and evaporation. A mixed segmentation model for end-members was used to determine the proportion of the contributions of different water sources to the target water body. The proportions of precipitation, supra-permafrost water, and glacier and snow meltwater for the mainstream were 41.70%, 40.88%, and 17.42%, respectively. The proportions of precipitation, supra-permafrost water, and glacier and snow meltwater were 33.63%, 42.21%, and 24.16% for the river in the glacier permafrost area and 20.79%, 69.54%, and 9.67%, respectively, for that in the permafrost area. The supra-permafrost water was relatively stable during the different ablation periods, becoming the main source of runoff in the alpine region, except for precipitation, during the ablation period.

Keywords: River water, stable isotope, ablation period, source region, Yangtze River

1. Introduction

Liquid precipitation, glaciers, snow, and permafrost in cold regions are important components of hydrological processes, serve as a key link in the water cycle, and are amplifiers and indicators of climate change (Yang et al., 2012; Chang et al., 2015; Li et al., 2016a; 2016b; 2018). They are not only important as the recharge sources of water in river basins but are also important resources to support regional development (Halder et al., 2015; Lafrenière et al., 2019). The temporal and spatial variations of runoff components are of great significance for water levels during wet and dry years in terms of ecological protection and the distribution of water resources (Wang et al., 2012; Pan et al., 2017; Mu et al., 2018). Therefore, the study on the composition change of runoff and its hydrological effect in cold areas can not only consolidate theories on runoff research, prediction, and adaptation, but also have important practical significance for construction, industry, and agriculture in cold regions (Wang et al., 2009; 2017; Wang et al., 2019).

The stable isotope tracer technique has become an important research method in hydrology. In recent years, the response of hydrological processes to climate change in cold regions has become a hot topic in the field of global change, which has greatly promoted the application of the stable isotope and chemical ion tracing methods in the analysis of runoff in cold regions (Li et al., 2015; 2019; Qu et al., 2017; Zhu et al., 2019). Liu et al. (2004) systematically studied the contribution of glacier and snow meltwater to runoff in a cold area in Colorado, USA. It was found that the contribution of glacier and snow meltwater to runoff in spring was as high as 82%.

Boucher and Carey (2010) systematically studied runoff segmentation in permafrost basins. Maurya et al. (2011) found that the average contribution of meltwater to runoff was 32% in typical glacial basins on the southern slope of the Himalayas. The application of the stable isotope tracer method in the analysis of runoff components in the cold regions of China has been relatively small. Gu and Longinelli (1993) first used $\delta^{18}O$ as a tracer in the Urumqi River in the Tianshan Mountains. The recharge water source can be separated into rainfall, snow meltwater, groundwater, and ice melt water. The results showed that groundwater and snow melt water were the major recharge sources of the Urumqi River in different periods and locations. Since then, Kong and Pang (2012) have studied the contribution of meltwater to runoff and its climatic sensitivity in two typical glacial basins in the Tianshan Mountains. The composition of runoff from the Tizinafu River in the Tianshan Mountains shows that the average contribution of snow melt water is 43% (Fan et al., 2015). The contribution of glacier and snow meltwater to runoff in the Baishui River in the Yulong Snow Mountains was 53.4% in summer (Pu et al., 2013). A study of the Babao River and the Hulugou basin in the Qilian Mountains showed that different water sources were fully mixed into groundwater before recharging rivers in this alpine cold region, and that the contribution of meltwater in the cryosphere to runoff in the cold region was as high as 33% (Li et al., 2014a; 2014b). Although these studies determined the contribution of precipitation and glacier and snow meltwater to runoff in the cold regions, they neglected the contribution of supra-permafrost water to runoff and its impact on hydrological processes (Prasch et al., 2013; Lutz et al.,

2014). On the one hand, it increases the uncertainty of runoff analysis in the cold regions. On the other hand, it is difficult to comprehensively evaluate the impact of components on the runoff process and the hydrological effects in cold regions.

The source of the Yangtze River, which is a typical alpine frozen soil area, is an important ecological barrier and a protected water source in China (Liang et al., 2008; Li et al., 2017). The regional climate shows a significant warm and wet trend against the background of global climate change. The regional climate shows a significant warm and wet trend against the background of global climate change. So regional evapotranspiration increases and ice and snow resources exhibit an accelerating melting trend (Kang et al., 2007; Wang et al., 2019). The increasing of ground temperature can cause it to melt significantly. The active layer becomes thicker and degenerates remarkably (Shi et al., 2019). Given this background, the temporal and spatial patterns, mechanisms, and influences of precipitation, glacier and snow meltwater, meltwater in the active layer, and groundwater in the region undergo profound changes and impact runoff processes (Wu et al., 2015). These significant impacts and their hydrological effects on the entire basin have gradually become prominent.

In summary, due to the lack of data and the difficulty of observation and sampling in cold regions, current studies have paid more attention to the study of hydrological processes and water cycle characteristics at the watershed scale from the macroscopic

119 point of view. However, there is a lack of in-depth study on the mechanism of the
120 temporal and spatial variations of runoff components from the microscopic point of
121 view, and the understanding of its hydrological effects is still in the exploratory stage.
122 At present, although stable isotope tracer techniques have been applied to the analysis
123 of runoff in cold regions, most of the current studies are limited to the assessment of
124 the contribution and impact of glacier and snow melt water but neglect the significant
125 role of liquid precipitation increase and melt water in the active layer. The results in a
126 lack of systematic understanding of the hydrological effects of runoff composition
127 changes in cold regions. Meanwhile, different types of tributaries in runoff-producing
128 areas are the key to runoff-producing processes and are the main links to
129 understanding hydrological processes in cold regions. It is urgent to develop an
130 understanding of how runoff is produced. In addition, the current study of
131 hydrological processes in the source area of the Yangtze River focuses on the
132 variation in runoff itself and its response mechanism to climate change, lacking
133 in-depth analysis of runoff components and its hydrological effects. Therefore, taking
134 the source area of the Yangtze River as an example, we conduct a study into the
135 temporal and spatial variations of isotopes in different tributary rivers under the
136 background of climate warming and their influencing factors by using the methods of
137 field observation, experimental testing, stable isotope tracing, and analytical modeling
138 of end-element mixed runoff. Based on the conversion signals of stable isotopes in
139 each link of the runoff process, at first, this study further explores the hydraulic
140 relations, recharge-drainage relations and their transformation paths, and the processes

of each water body. Furthermore, this study determines the composition of runoff, quantifies the contribution of each runoff component to different types of tributaries. Finally, this study analyzes the hydrological effects of the temporal and spatial variation of runoff components. On the one hand, the research results can reveal the evolution mechanism of runoff in cold regions under the background of climate warming. On the other hand, it provides parameter support and a theoretical basis for the simulation and prediction of runoff changes in cold regions, and then provides a scientific basis for a more systematic understanding of the hydrological effects caused by underlying surface changes in cold regions, ultimately providing decision-making basis for the rational development and utilization of water resources in river basins.

2. Data and Methods

2.1 Study area

The source region of the Yangtze River is located in the hinterland of the Tibetan Plateau (Fig. 1). It is an important ecological barrier and water conservation region in China. The southern boundaries are the Tanggula Mountains and Sederi Peak, which contain the watersheds of the Salween River and Lantsang River, respectively. The mean altitude reaches 4000 m above sea level with a decreasing elevation from west to east (Yu et al., 2013) that covers an area of approximately 138,000 km^2, ~7.8% of the total area of the Yangtze River Basin. Most tributaries start from glaciers, and form very dense drainage networks, such as those of the Chumaer River in the north, Tuotuohe River in the middle, and Dangqu River in the south (Pu, 1994). The glaciers

in the study area are mainly distributed along the north-oriented slopes of the Tanggula Mountains and Sedir Mountains and the south-oriented slopes of the Kunlun Mountains, with a total area of 1496.04 km^2 (Yao et al., 2014). The permafrost has a thickness of 10 – 120 m, which accounts for 77% of the total basin area, and most surface soils are frozen during winter and thaw in summer, and active layer thicknesses range from 1–4 m (Gao et al., 2012). Annual average temperatures range from 3 – 5.5°C. The annual precipitation is 221.5 – 515 mm (Yu et al., 2014). The mean annual precipitation varies considerably over the reserve, and ~80% of the annual precipitation occurs during summer, with the highest precipitation occurring in August.

2.2 Sample Collection

This study mainly collects precipitation, glacier and snow melt-water, supra-permafrost water and river water to systematic analysis the recharge relationship between precipitation, glacier and snow melt-water, supra-permafrost water and river water in the source area of the Yangtze River. In this study, the initial ablation period is from May to June, the strong ablation period is from July to August, and the end ablation period is from September to October. In order to analyze the influence of meteorological factors on the stable isotope in river water, samples were collected once per week at the ZMD and TTH stations throughout the sampling period. A total of 201 river water samples were collected in this study. The specific sampling process is as follows:

River water: In order to analysis the spatial and temporal characteristic of stable isotope of river water in mainstream (25 samples) and major tributary (including river in glacier permafrost area (105 samples) and river in permafrost area (167 samples)) in the study area, All of river water samples around the traffic routes in the source area of the Yangtze River were collected in initial ablation in 2016 (48 samples), ablation in 2016 (88 samples), end ablation in 2016 (45 samples), ablation in 2017 (55 samples) and ablation in 2018 (61 samples) (Fig.1).

Glacier and snow melt-water: This paper researched the hydrochemistry characteristic of melt-water in Cryosphere (Yuzhu peak Glacier, Geladandong Glacier and Dongkemadi Glacier) through collected water samples by fixed-point sampling from June to September in 2016 and 2017. The samples were collected once every 10 days at the glacier front during the ablation period. The sampling time is at 14 o'clock per day. The sampling location is in hydrological section at the end of the glacier.

Supra-permafrost water: Supra-permafrost water is the most widely distributed groundwater type in the SRYR, and it is mainly stored in the permafrost active layer (Li et al.,2018). The hydrochemistry characteristic of supra-permafrost water in the study area this paper collected water samples by comprehensive sampling from June to September in 2016 and 2018. The sampling process is manual operation. At first, a 2-m deep profile of the permafrost active layer was dug at each of the sampling points.

Then, the collection of the water samples are immediately filtered with 0.45 um Millipore filtration membrane. Then, samples were poured the filtered into a clean polyethylene bottle.

Precipitation: precipitation samples were collected at Zhimenda Hydrological Station (ZMD) at the mountain pass of the source area of the Yangtze River, Qumalai Meteorological Station(QML) in the middle reaches of the source area and Tuotuo River Meteorological Station(TTH) in the upper reaches of the source area. The sampling period extended from April 1, 2016 to October 31, 2018.

Before analysis, all samples were stored at 4ºC in a refrigerator without evaporation. Precipitation and surface water samples were analyzed for $\delta^{18}O$ and δD by means of laser absorption spectroscopy (liquid water isotope analyzer, Los Gatos Research DEL-100, USA) at the Key Laboratory of Ecohydrology of Inland River Basin, Northwest Institute of Eco-Environment and Resources, CAS. The results are reported relative to the Vienna Standard Mean Ocean Water (VSMOW). Measurement precisions for $\delta^{18}O$ and δD were better than 0.5‰ and 0.2‰, respectively. Field measurements included pH, dissolved oxygen (DO), electrical conductivity (EC), and water temperature.

2.3 End-Member Mixing Analysis

Hooper (2003) introduced the end-member mixing analysis (EMMA) using

chemical/isotopic compositions in waters. The techniques involve graphical analyses, in which chemical and isotopic parameters are used to represent the designated end members. Tracer concentrations are constant in space and time. Essentially, the composition of the water changing can be considered as a result of intersections during its passage through each landscape zone. Tracers can be used to determine both sources and flow paths. The EMMA tracer approach has been a common method for analyzing potential water sources contributing to stream flow (Li et al, 2014a; 2016a). Here in a three end-member mass-balance mixing model is employed to calculate the contribution of up to three water sources in stream water, such as the following:

$$X_S=F_1X_1+F_2X_2+F_3X_3 \quad (1a)$$

$$Y_S=F_1Y_1+F_2Y_2+F_3Y_3 \quad (1b)$$

In Eq. (1), X and Y represent concentrations of two types of different tracers. In this study, $\delta^{18}O$ and deuterium excess were chosen for comparison. The subscripts represents stream water sample, and 1, 2, and 3 represent water from the respective contribution of three respective source waters (end members) to stream water. The fraction of each end-member is denoted by F. The solutions for F_1, F_2, and F_3 in regards to tracer concentrations in Eq. (1) can be given as:

$$F_1=[(X_3-X_S)/(X_3-X_2)-(Y_3-Y_S)/(Y_3-Y_2)]/[(Y_1-Y_3)/(Y_3-Y_2)-(X_1-X_3)/(X_3-X_2)] \quad (2a)$$

$$F_2=[(X_3-X_S)/(X_3-X_1)-(Y_3-Y_S)/(Y_3-Y_1)]/[(Y_2-Y_3)/(Y_3-Y_1)-(X_2-X_3)/(X_3-X_1)] \quad (2b)$$

$$F_3=1-F_1-F_2 \quad (2c)$$

This method has been used by previous study (Li et al.,2014b; 2015; 2016b). This study also used this method to evaluate the contribution of possible sources to the river water.

2.4 Uncertainty in hydrograph separation

The uncertainty of tracer-based hydrograph separations can be calculated using the error propagation technique (Genereux, 1998; Klaus & McDonnell, 2013). This approach considers errors of all separation equation variables. Assuming that the contribution of a specific streamflow component to streamflow is a function of several variables c1, c2, ⋯, cn and the uncertainty in each variable is independent of the uncertainty in the others, the uncertainty in the target variable (e.g.,the contribution of a specific streamflow component) is estimatedusing the following equation (Genereux, 1998; Uhlenbrook & Hoeg,2003):

$$W_{fx} = \sqrt{\left(\frac{\partial z}{\partial c_1} W_{c1}\right)^2 + \left(\frac{\partial z}{\partial c_2} W_{c2}\right)^2 + \cdots + \left(\frac{\partial z}{\partial c_n} W_{cn}\right)^2}, \quad (3)$$

where W represents the uncertainty in the variable specified in the ubscript. fx is the contribution of a specific streamflow component x to streamflow. The software package MATLAB is used to apply equation 3 to the different hydrograph separations in this study.

3. Results

3.1 Temporal Variation

As shown in Fig. 2, stable isotope characteristics of $\delta^{18}O$ and d-excess was different during different ablation for the different types of runoff. For the mainstream, the $\delta^{18}O$ in initial ablation was higher than end ablation, while the ablation period was the lowest. But $\delta^{18}O$ in ablation period showed decreasing trend from 2016 to 2018. With

the same as $\delta^{18}O$, d-excess in the different ablation periods was different (Fig. 2a, d). For the river in the glacier permafrost area, the order of $\delta^{18}O$ for the different ablation periods and the ablation period from 2016 to 2018 was the same as the mainstream order, but the values of $\delta^{18}O$ were different for the mainstream (Fig. 2b, e). For the river in the permafrost area, the variation $\delta^{18}O$ for the different ablation periods and ablation from 2016 to 2018 was the same as for the mainstream and the river in the glacier permafrost area. However, the order of d-excess was different for the river in the permafrost area and the glacier permafrost area (Fig. 2c, f). In general, the $\delta^{18}O$ in the mainstream was more negative than those in the rivers in the glacier permafrost and permafrost areas. These results may be due to the fact that the highest runoff was for the mainstream and that the effects of dilution result in lower isotope values. However, the $\delta^{18}O$ in the river in the glacier permafrost area was more positive than those in the mainstream and the river in the permafrost area. The effect of evaporation could explain these results and the change in d-excess could also demonstrate the same.

3.2 Spatial Variation

To analyze the spatial variation of $\delta^{18}O$ based on the different ablation periods in 2016 and ablation from 2016 to 2018, spatial interpolation of all river water samples in the study area was performed using ArcGIS. The results are shown in Fig. 3. The $\delta^{18}O$ value in the north-central region of the study area was more positive than those in other regions. In the southeastern part of the study area, especially the QML, ZMD,

and Tanggula Mountains, the values were more negative during the initial ablation period. The area of positive ablation during the ablation period, which was concentrated mainly in the northeast part of the study area, was larger than that during the initial ablation. The other regions, except some areas in the southwest, turned positive. The area of positive ablation was largest during the final of the different ablation periods in 2016; all areas, except some in the eastern region of the study area, were positive (Fig. 3). The area of positive ablation in the central and northern regions began to expand in 2017 compared to the area of ablation in 2016. Furthermore, the area of negative ablation appears mainly in the southeastern and southwestern portions of the study area. However, the positive ablation area was also concentrated in the central and northern regions in 2018 and it was greater than it was in 2016 and 2017. Meanwhile, the negative ablation area appeared mainly in the southeastern and southwestern portions of the study area, but it was smaller than in 2016 and 2017. These results may be related to evaporation, possible recharge sources, or meteorological factors. These results were comprehensive and influenced by meteorological factors and the type and proportion of recharge sources. The evaporation effect was strong in the central and northern regions, which were also the major glacier and permafrost regions. The southeastern region was the downstream area where all runoff converged; thus, the dilution effect led to a more negative $\delta^{18}O$ here. Moreover, the Tanggula Mountains, with altitudes higher than those in other regions, were located southwest of the study area; thus, evaporation had a low influence on this region and the oxygen stable isotopes were more negative.

Just as with the spatial distribution of $\delta^{18}O$, there was a significant spatial distribution of d-excess in the study area (Fig. 4). Compared to the spatial distribution of $\delta^{18}O$, the d-excess in the central and northern regions were lower than those in the other regions. However, d-excess was higher in the latter, especially in the southwestern regions and in the southeastern regions during the initial ablation period. The lower area begin to expand during the ablation period in 2016, while the central and northeastern regions and the Tanggula Mountains were greater. Meanwhile, the negative ablation area continued to expand during the end ablation period; ablation was greater only in the southeastern part of the study area. However, all regions except for areas in the eastern region where the ablation was low during the ablation period in 2017 exhibited high ablation especially Tanggula Mountains. Moreover, the lower ablation regions appeared mainly in the central and southeastern regions of the study area; values were higher in the other regions, especially in the Tanggula Mountains and the northeast. The spatial distribution of d-excess also confirmed the spatial distribution of the oxygen stable isotope because evaporation resulted in the enrichment of isotopes and led to a reduction in d-excess.

In general, the influence of evaporation on the isotope and d-excess was only manifested in some places, such as the central and northern parts of the study area, in the initial ablation and the ablation periods. However, the influence of evaporation on the isotope and d-excess was manifested in most places, except the southeast of the

study area. Meanwhile, these results also indicated that there may be a hysteresis for the influence of meteorological factors on isotopes and d-excess. On the one hand, river water was the result of the final convergence of various recharge sources that include precipitation, supra-permafrost water, and glacier and snow meltwater. On the other hand, meteorological factors directly affected the main recharge sources of river water.

As shown in Fig. 5, there was a significant difference in the variation of $\delta^{18}O$ and d-excess with altitude for the mainstream, the river in the glacier permafrost area, and the river in the permafrost area of the study area. For the mainstream, the oxygen stable isotope showed a decreasing trend, with increases in altitude, during the ablation periods in 2016 and 2018. In other words, the altitude effect only appeared in the ablation periods during these two years and had values of −0.16‰/100 m ($p < 0.05$) and −0.14‰/100 m ($p < 0.05$), respectively. However, $\delta^{18}O$ showed an increasing trend with an increase in altitude during the initial and end ablation periods in 2016 and ablation period in 2017. The anti-altitude effects of the initial and end ablation periods in 2016, and ablation period in 2017, were 0.11‰/100 m ($p < 0.05$), 0.13‰/100 m ($p < 0.01$), and 0.04‰/100 m ($p < 0.05$), respectively. For the phenomenon of anti-altitude effect, the following reasons can explain this phenomenon: on the one hand, in the source area of the river, the stable isotope concentration of precipitation and glacier snow meltwater is relatively low and the value of groundwater in the permafrost active layer is relatively positive due to the

370 influence of soil evaporation; On the other hand, the more the inflow of precipitation,
371 the greater the contribution of precipitation. So there is an obvious diluting effect of
372 biotin, which makes the concentration more negative. D-excess showed a decreasing
373 trend during the initial and end ablation periods in 2016 and a significant increasing
374 trend in the ablation period from 2016 to 2018. For the river in the glacier
375 permafrost area, $\delta^{18}O$ showed a decreasing trend with increase in altitude during the
376 ablation periods in 2016 and 2018, but the ablation in 2018 was not significant. The
377 altitude effect was −0.66‰/100 m ($p < 0.05$) and −0.15‰/100 m ($p > 0.05$),
378 respectively, during the former two periods. Moreover, a significant anti-altitude
379 effect of 0.47‰/100 m ($p < 0.05$), 0.67‰/100 m ($p < 0.05$), and 0.97‰/100 m
380 ($p < 0.05$), appeared in the initial and end ablation periods in 2016 and ablation
381 period in 2017, respectively. Just as with the mainstream, d-excess showed a
382 decreasing trend in the initial and end ablation periods in 2016 and an increasing trend
383 in the ablation from 2016 to 2018. For the river in the permafrost area, $\delta^{18}O$ showed
384 a decreasing trend with an increase in altitude in the initial ablation period and
385 ablation period in 2016, with an altitude effect of −0.38‰/100 m ($p < 0.05$) and
386 −0.12‰/100 m ($p > 0.05$), respectively. However, $\delta^{18}O$ showed an increasing trend
387 with increase in altitude in the end ablation period in 2016 and the ablation periods
388 in 2017 and 2018, with an anti-altitude effect of 0.21‰/100 m ($p < 0.05$),
389 0.01‰/100 m ($p > 0.05$), and 0.68‰/100 m ($p < 0.05$), respectively. d-excess showed
390 an increasing trend with increase in altitude in the initial and end ablation periods in
391 2016 and ablation periods in 2016 and 2017. However, d-excess also showed a

392 decreasing trend with increase in altitude in the ablation period in 2018.

393

394 In summary, the altitude effect mainly appeared during ablation, whether it was in the
395 mainstream, the river in the glacier permafrost area, or the river in the permafrost area.
396 The altitude effects were higher for the river in the glacier permafrost area than for the
397 mainstream or the river in the permafrost area during the ablation period in 2016.
398 Meanwhile, the anti-altitude effect of the river in the glacier permafrost area was
399 higher than that of the other areas. The $\delta^{18}O$ during the initial and end ablation periods
400 in 2016 showed a significant anti-altitude effect for the mainstream and the river in
401 the glacier permafrost area; a significant altitude effect appeared during the initial
402 ablation period for the river in the permafrost area. These results may be due to the
403 comprehensive influence of possible recharge sources and different recharge
404 proportions caused by the influence of meteorological factors. This kind of
405 comprehensive influence is mainly due to the significant seasonality of climate factors
406 in the cold regions, which directly determines the types and contribution proportion of
407 possible recharge sources. Therefore, this result can not be said to be caused by any
408 one factor, but can only be explained by the comprehensive influence of possible
409 recharge sources and different recharge proportions caused by the influence of
410 meteorological factors.

411 **3.3 Evaporation Line**

412

413 The variations in the location of the evaporation line for river water during the
414 different ablation periods in 2016 and the ablation periods from 2016 to 2018 are

shown in Fig. 6. The slope and intercept of the LEL for river water showed an increasing trend from the initial to end ablation periods in 2016. The LEL in the initial ablation period was $\delta D = 6.59\delta^{18}O - 3.60$ ($p < 0.01$) and it was $\delta D = 6.88\delta^{18}O - 1.37$ ($p < 0.01$) during the ablation period. The LEL during the end ablation period was $\delta D = 7.39\delta^{18}O + 5.88$ ($p < 0.01$). These results indicate that the effect of evaporation on the stable isotopes in river water gradually weakened from the initial ablation to the end ablation periods. The slope and intercept of the LEL of river water during the ablation period in 2017 were lower than those in 2016. The LEL during the ablation period in 2017 was $\delta D = 6.59\delta^{18}O - 3.63$ ($p < 0.01$). However, whether the slope or the intercept of LEL of river water in 2018 was higher than that in 2016 and 2017, with the LEL was: $\delta D = 7.63\delta^{18}O + 5.82$ ($p < 0.01$). This phenomenon showed that the influence of evaporation on stable isotope levels was greatest during the ablation period in 2017, followed by that in 2016. In general, the lower slope and intercept indicate that the water body was affected by evaporation or non-equilibrium dynamic fractionation. This conclusion could also explain the results of this study.

3.4 Recharge Sources

The distribution of δD and $\delta^{18}O$ for river water among other water bodies are shown in Fig. 7 during the different ablation periods in 2016 and ablation from 2016 to 2018. The results of the distribution of δD and $\delta^{18}O$ of river water indicate the possible recharge sources of river water. However, the δD and $\delta^{18}O$ of river water, supra-permafrost water, glacier snow meltwater, and precipitation exhibited little

change during the initial ablation in 2016 (Fig. 7a, b). This phenomenon suggests that precipitation may be the major recharge sources for river water during the initial ablation. A plot of δD versus $\delta^{18}O$ for river and supra-permafrost water, glacier snow meltwater, and precipitation is shown in Fig. 7c. The δD and $\delta^{18}O$ values of glacier and snow meltwater from above the LMWL are the most negative compared to other water bodies. The stable isotope of supra-permafrost water was relatively more positive, located below the LMWL, confirming the influence of strong evaporation. The stable isotope of river water was close to the LMWL, and its concentration value was between precipitation, glacier and snow meltwater, and supra-permafrost water, reflecting that river water was recharged and affected by multi-source water in the study area. Moreover, the distribution of river water, glacier and snow meltwater, and supra-permafrost water also indicated that there was a hydraulic relationship between the source and target in the different ablation periods in 2016 and ablation from 2016 to 2018.

The mixed segmentation model of the end-member is used to determine the contribution proportions of different water sources to the target water. Owing to the two stable isotope concentrations in different water bodies have significant spatial and temporal differences, it can effectively distinguish different water bodies and their mixing relationships. The d-excess and $\delta^{18}O$ are used as tracers of the mixed segmentation model of the end-elements. As shown in Fig. 8, according to the locations of the different types of water and the distance from other water bodies,

460 which reflected the mixed recharge of three water bodies, supra-permafrost water was
461 the first end element, precipitation was the second end element, and glacier and snow
462 meltwater was the third end element. However, the different runoffs likely have
463 different recharge sources and different recharge proportions. The glacier permafrost
464 area river comprised glacier and snow meltwater more in the ablation period than in
465 other periods. Compared with the permafrost area river and the glacier permafrost
466 area river, the mainstream was governed by the supra-permafrost water in the initial
467 ablation period while containing nearly equal proportions of supra-permafrost water
468 and precipitation in the end ablation period. However, the mainstream received
469 significant contributions from all three end members in the ablation period from
470 2016 to 2018 and particularly in 2017.
471
472 The recharge proportions of precipitation, supra-permafrost water, and glacier and
473 snow meltwater at different altitudes are depicted in Fig. 9, from the mixed
474 segmentation model of the three end-members during the ablation periods mentioned
475 above. The recharge proportions of the three end members in the ablation periods
476 were significantly different. This may be due to the different effects of the runoff
477 recharge sources in different ablation periods, as well as the significant differences in
478 recharge and drainage relationships in the different ablation periods. The recharge
479 proportions of precipitation in the initial ablation in 2016, ablation in 2016, end
480 ablation in 2016, ablation in 2017, and ablation in 2018, obtained by calculating
481 the average contribution proportion from each altitude, were 28.71%, 44.41%,

44.60%, 42.53%, and 51.03%, respectively. Meanwhile, the recharge proportions of supra-permafrost water in the initial ablation in 2016, ablation in 2016, end ablation in 2016, ablation in 2017, and ablation in 2018 were 55.38%, 36.51%, 40.21%, 37.56%, and 28.87%, respectively. The recharge proportions of glacier and snow meltwater in the initial ablation in 2016, ablation in 2016, end ablation in 2016, ablation in 2017, and ablation in 2018 were 15.91%, 19.08%, 15.19%, 19.90%, and 20.09%, respectively. The recharge proportion of precipitation decreased with increase in altitude in the initial ablation, while the proportion of supra-permafrost water and glacier and snow meltwater exhibited an increasing trend with increase in altitude. However, the recharge proportion of the supra-permafrost water was higher than that of precipitation or glacier and snow meltwater, and also showed a decreasing trend from low to high altitude in the end ablation in 2016. The proportion of glacier and snow meltwater increased with increase in altitude, but the recharge proportion of supra-permafrost water was stable with the change in altitude in the end ablation in 2016. The trend of precipitation and glacier and snow meltwater for the ablation was the same as that for the initial and end ablation. However, the recharge proportion of precipitation was higher than the proportion of supra-permafrost water and glacier and snow meltwater in the ablation period. Meanwhile, the recharge proportion of glacier and snow meltwater in ablation was higher than that in the initial and end ablation period. In general, the recharge of supra-permafrost water to runoff was stable, whether in the different ablation periods in 2016 or the ablation from 2016 to 2018. However, the proportion of supra-permafrost water was relatively low, mainly

504 due to the larger runoff during the ablation period.

505

506 Using the approach shown in Equation (3), the uncertainty originating from the
507 variation in the tracers of components and measurement methods could be calculated
508 separately (Uhlenbrook & Hoeg, 2003; Pu et al., 2013). According to the calculations
509 made using Equation (3), the uncertainty was estimated to be 0.07 for the three -
510 component mixing model in the study region. The uncertainty terms for
511 supra-permafrost water accounted for more than 50.0% of the total uncertainty,
512 indicating that the $\delta^{18}O$ and δD variations of supra-permafrost water accounted for the
513 majority of the uncertainty. Although there is some uncertainty for hydrograph
514 separation, isotope-based hydrograph separations are still valuable tools for evaluating
515 the contribution of meltwater to water resources, and they are particularly helpful for
516 improving our understanding of hydrological processes in cold regions, where there is
517 a lack of observational data.

518

519 **4. Discussions**

520

521 **4.1 Meteorological Factors**

522

523 To further explain the reason for the variation in temporal and spatial characteristics
524 of stable isotopes and LEL, this study includes the analysis of the monthly change in
525 precipitation, temperature, relative humidity, and evaporation during the sampling
526 period (from January 2016 to December 2018). The results are shown in Fig. 10. The
527 average of the precipitation was 371.9 mm during the sampling period, and the

precipitation in the ablation period accounted for 78.87%. The average of the temperature, relative humidity, and evaporation during the sampling period were −1.42 °C, 52.20%, and 4.14 mm, respectively. However, the average of the temperature, relative humidity, and evaporation during the ablation period were 8.04 °C, 66.47%, and 5.57 mm, respectively.

More importantly, the precipitation during the initial, total, and end ablation periods in 2016, and the ablation periods in 2017 and 2018, were 50.40 mm, 107.90 mm, 42.90 mm, 70.60 mm, and 119.00 mm, respectively. For precipitation, the isotope levels tend to decrease with the increase in rainfall; Precipitation is also the major source of water for all water bodies (Maurya et al., 2011; Pu et al., 2013; Li et al., 2014b; 2015; 2016a; 2018; Pan et al., 2017) and, in general, more precipitation resulted in a greater dilution effect. A more negative $\delta^{18}O$ appeared in the ablation period in 2016 whether in all three study areas given the change in $\delta^{18}O$ (Fig. 2). This result showed that dilution does not only play an important role in the precipitation effect; it also affects river water. However, the dilution effect was also significant when precipitation was the major recharge source for river water (Abongwa and Atekwana, 2018; Li et al., 2015).

Temperature for the initial, total, and end ablation periods in 2016, and the ablation periods in 2017 and 2018, were 6.82 °C, 9.58 °C, 3.77 °C, 9.47 °C, and 11.09 °C, respectively. For atmospheric precipitation, the lower the temperature was, the higher

the condensation degree of water vapor exhibited and the lower the isotope content in precipitation. Therefore, there is a positive correlation between the stable isotope and temperature in precipitation (Li et al., 2016a). However, the influence of temperature on the stable isotope of river water was not significant from the variation in river water isotope during the different ablation periods. However, the variation trend of the stable isotope of river water in the ablation period from 2016 to 2018 was similar to that for the change in temperature. Meanwhile, the variation trend of d-excess can also be confirmed by this analysis (Fig. 2).

Relative humidity in the initial ablation, ablation, and end ablation periods in 2016 and the ablation periods in 2017 and 2018 were 60.07%, 63.16%, 70.57%, 63.39%, and 63.48%, respectively. When the relative humidity is low, the dynamic fractionation increases and the slope decreases, and vice versa. The variation trend of the slope of the LEL for the different ablation periods in 2016 was the same as that for the change in relative humidity (Fig. 6). Meanwhile, the intercept of the LEL for the different ablation periods in 2016 also showed the same trend.

Evaporation in the initial ablation, ablation, and end ablation periods in 2016 and ablation periods in 2017 and 2018 were 6.69 mm, 6.96 mm, 4.02 mm, 6.48 mm, and 6.02 mm, respectively. The stable isotopes of hydrogen and oxygen in river water are comprehensively affected by the evaporation process, runoff change, precipitation recharge, glacier and snow meltwater recharge and supra-permafrost water in cold

572 regions. During the process of evaporation, lighter water isotopes are separated
573 preferentially from the surface of water while heavier isotopes are enriched in the
574 remaining water body. Evaporation enriches the oxygen and hydrogen stable isotopes
575 and reduces excess deuterium (Li et al., 2015; 2018). The trend in the oxygen isotope
576 in the ablation periods from 2016 to 2018 was the same as that for the change in
577 evaporation (Fig. 2). Meanwhile, the spatial distribution of $\delta^{18}O$ and d-excess also
578 responded to this change (Fig. 3, 4).
579
580 To further analyze the influence of meteorological factors on the stable isotope, the
581 correlation analysis between meteorological factors and the monthly value of $\delta^{18}O$
582 and d-excess, which showed continuous observations at two fixed-point stations was
583 analyzed (Table 1), and the results are shown in Table 1. There was a significant
584 negative correlation between precipitation and $\delta^{18}O$ at the 0.01 level (2-tailed), while
585 a significant positive correlation between precipitation and d-excess was also present.
586 More interestingly, just as with precipitation, a significant negative correlation
587 appeared between $\delta^{18}O$ and temperature, relative humidity, and evaporation, with
588 coefficients of −0.671, −0.555, and −0.636, respectively. Meanwhile, a significant
589 positive correlation occurred between d-excess and temperature, relative humidity,
590 and evaporation, with coefficients of 0.602, 0.524, and 0.533, respectively. This
591 results indicated that the direct influence of meteorological factors on stable isotopes
592 of river water was significant and definite.
593

Hydrogen and oxygen isotope compositions in river water are the result of the combined effects of the isotopes making up present in precipitation, glacier and snow meltwater, and supra-permafrost water as well as evaporative fractionation (Li et al., 2015). The main influential hydrometeorological factors include precipitation, temperature, relative humidity, and evaporation. On the whole, river water isotopes were not influenced by a single factor; instead, they were based on the comprehensive influence of many factors in the cold regions. The influence of meteorological factors on different types of river water (mainstream, rivers in glacier permafrost areas, and rivers in permafrost areas) showed that apart from their directly influences, each factor indirectly affected the river water recharge source. This indirect influence was mainly felt on precipitation, glacier, snow, and permafrost.

4.2 Hydrological processes

To systematically quantify the main recharge sources of different types of runoff in the alpine regions, the possible sources and recharge proportions of runoff of different types in different ablation periods were deeply analyzed by using the mixed segmentation model of the three end-members in this study. The conceptual model map of the recharge form and proportion of the river water in the different ablation periods is shown in Fig. 11.

For the river in the glacier permafrost area, there was a significant difference in the

617 recharge proportion in the runoff area, in which there were several glaciers and
618 permafrost in the basin, and other areas during the various ablation periods. The
619 proportion of recharge from precipitation during the initial, total, and end ablations in
620 2016, the ablation in 2017, and the ablation in 2018 were 27.69%, 33.71%,
621 32.38%, 33.21%, and 41.48%, respectively. However, the proportion of
622 supra-permafrost water in the initial, total, and end ablations in 2016, the ablation in
623 2017, and the ablation in 2018 were 54.68%, 35.96%, 46.38%, 37.39%, and 36.63%,
624 respectively. The proportions of glacier and snow meltwater in the initial, total, and
625 end ablations in 2016, the ablation in 2017, and the ablation in 2018 were 17.63%,
626 30.33%, 21.24%, 29.39%, and 22.19%, respectively. These results show that
627 supra-permafrost water was the important recharge source for runoff during the initial
628 and end ablation periods. The proportion of supra-permafrost water was 50.53%
629 during the initial and end ablation periods. It was also the next highest source of
630 runoff recharge, next to precipitation, during the ablation from 2016 to 2018; the
631 proportions were 36.13% and 36.66%, respectively. The recharge proportions for
632 glacier and snow meltwater was higher during the ablation period than in the initial
633 and end ablation periods, at 19.44% and 27.30%, respectively.
634
635 For permafrost area river, the runoff area only with permafrost and no glacier in the
636 basin, there was also an obvious difference for the recharge proportion in different
637 ablation period. Compared with the glacier permafrost area river the recharge
638 proportion of supra-permafrost water was higher for permafrost area river than that

for the glacier permafrost area river (42.21%). The recharge proportion of supra-permafrost water was 69.54%. With the same as the glacier permafrost area river, the supra-permafrost water was the important recharge sources to runoff in the initial and end ablation, and the proportion was 80.97% in the initial and end ablation period. Meanwhile, the proportion of supra-permafrost water was 61.92% in the ablation period. The proportion was higher than that for precipitation (24.13%) in the ablation period. In general, the supra-permafrost water was the major recharge source for the permafrost area river in the different ablation periods in the study area. Meanwhile, the glacier and snow meltwater had little contribution to the permafrost area river in the initial and end ablation periods.

For the mainstream, the recharge proportions for precipitation during the initial, total, and end ablations in 2016, the ablation in 2017, and the ablation in 2018 were 28.67%, 48.35%, 43.18%, 46.97%, and 41.33%, respectively. The proportion was 35.93% in the initial and end ablation periods and 45.55% in the ablation period. However, the proportions of supra-permafrost water during the initial, total, and end ablation in 2016, the ablation in 2017, and the ablation in 2018 were 52.37%, 33.52%, 42.61%, 39.68%, and 38.21%, respectively. The proportion was 47.49% during the initial and end ablation periods and 36.47% during the ablation period. These results indicate that, for the study area, the supra-permafrost water was the major recharge source for the mainstream in the first two of these ablation periods while precipitation was the major recharge source for the mainstream in the ablation

661 period. The proportions of glacier and snow meltwater during the initial, total, and
662 end ablation in 2016, the ablation in 2017, and the ablation in 2018 were 18.96%,
663 20.13%, 14.21%, 13.35%, and 20.46%, respectively. The proportion of glacier and
664 snow meltwater for the mainstream (16.59%) was higher than that for the river in the
665 permafrost area (3.25%) but lower than that for the river in the glacier permafrost area
666 (19.44%) during the initial and end ablation periods. The former proportion was also
667 higher than that for the river in the permafrost area (17.98% vs 13.95%) but lower
668 than that for the river in the glacier permafrost area (27.30%) during the ablation
669 period.
670
671 The hydrological process in cold regions has one particularity. The low permeability
672 in permafrost layer and the freeze-thaw depths of the soil reduces soil infiltration (Wu
673 et al., 2015; Wang et al., 2019). Therefore, the rapid replenishment of meltwater by
674 runoff results in a difference in the runoff generation mechanism in the permafrost
675 and non-permafrost regions (Yang et al., 2010; Li et al., 2018). Moreover, because the
676 freeze-thaw depths of the soil changes with annual fluctuations in temperature, there
677 is an effect on soil water storage capacity that results in a difference in the runoff
678 generation mechanism during different ablation periods (Wang et al., 2019). Wang et
679 al. (2008) also found that the seasonal distributions and variations in rainfall runoff in
680 the permafrost basin were controlled by the freeze-thaw process because of the
681 impermeable nature of the freeze-thaw front and permafrost layer. During the initial
682 ablation period, the supra-permafrost water—whether in the mainstream, the river in

683 the glacier permafrost area, or the river in the permafrost area—was the major
684 recharge source. During the ablation period, precipitation was the main source of
685 runoff recharge, followed by supra-permafrost water. Although there was little
686 difference the proportion of precipitation and supra-permafrost water during the
687 ablations from 2016 to 2018, precipitation was the major recharge source of runoff in
688 this period. Supra-permafrost water was the main source of runoff recharge in the end
689 ablation period, just as it was in the initial ablation period. In summary, runoff in the
690 cold region during the different ablation periods was mainly composed of runoff from
691 rainfall, meltwater, and supra-permafrost. Because of the inherent seasonal variation
692 in precipitation, there were significant changes in precipitation during the different
693 ablation periods. Glacier and snow meltwater was also greatly affected by climatic
694 factors during the different ablation periods, while the supra-permafrost water was
695 relatively stable; the latter became the main source of runoff supply, except for
696 precipitation, in the alpine region. Thus, with the changes that the low temperatures
697 made in the physical properties of the underlying surface, the change in the
698 permafrost had the most significant effect on the hydrological process in cold regions.
699
700 **4.3 Hydrological significance of permafrost**
701
702 The source region of the Yangtze River is a typical permafrost area. The permafrost
703 area is 107619.13 km^2, which accounting for 77% of the total area. The seasonal
704 frozen soil is mainly distributed in the valley area, with an area of 30754.34 km^2.
705 Field observation and research confirmed that most of the precipitation in permafrost

area is frozen on the ground or used to recharge the deficit of soil water, and does not directly form runoff in permafrost area. Under the background of permafrost degradation, the area of permafrost is gradually shrinking and the thickness of permafrost is gradually decreasing with the increase of the thickness of active layer. The degradation of ice rich permafrost in the cold regions has an important contribution to the development of surface runoff and hot karst lakes. Due to the decrease of permafrost water storage capacity in the Qinghai Tibet Plateau, the availability of water resources will be reduced in dry season, and the increase of water melting may lead to the increase of flood risk, and the resilience of ecosystem will be reduced through the seasonal changes of river flow and groundwater abundance. All these changes will affect the water resources balance and sustainable development of the Qinghai Tibet Plateau, including the headwaters of major rivers in Asia, including the Yellow River, the Yangtze River, the Salween River, the Mekong River, the Brahmaputra River, the Ganges River, the Indus River, the Ili River, the Tarim River, the Erqis River and the Yenisei River Rivers, these rivers provide fresh water resources for the survival of about 2 billion people.

In brief, the freeze-thaw of soil in the active layer plays an important role in controlling river runoff. The increase in melting depth leads to a decrease in the direct runoff rate and slow dewatering process. The two processes of runoff retreat are the result of soil freeze-thaw in the active layer. Permafrost has two hydrologicalfunctions: on the one hand, permafrost is an impervious layer, and it has the function of

preventing surface water or liquid water from infiltrating into deep soil; on the other hand, it forms a soil temperature gradient, which makes the soil moisture close to the ice cover. Therefore, changes in the soil water capacity, soil water permeability, and soil water conductivity, as well as the redistribution of water in the soil profile, are caused by the freeze-thaw of the active layer. The seasonal freeze-thaw process of the active layer directly leads to seasonal flow changes in surface water and groundwater, which affects surface runoff. Climate warming is the main driving force in the degradation of cold ecosystems (Wang et al., 2009; Wu et al., 2015; Li et al., 2018; Wang et al., 2019). More importantly, under the background of intense melting, the melting water of the cryosphere has had a significant impact on the hydrological process in the cold region. The hydrological function of groundwater in the permafrost active layer should be paid more attention, especially in the cold region where glaciers are about to subside, its hydrological function needs to be recognized. The stable isotope characteristics of the cryosphere are more complex than other regions, and its mechanism is more complex Further research is needed.

5. Conclusions

Through systematically analysis of the characteristics of $\delta^{18}O$, δD, and d-excess of river water in the different ablation periods in 2016 and the ablation periods from2016 to 2018, the results were as follows. The temporal and spatial characteristics of stable isotopes of river water were significant in the study area. The δ18O in mainstream was more negative than that in the glacier permafrost area river and permafrost area

751 river. The influence of evaporation on isotope and d-excess is only prevalent in some
752 places, such as the central and northern parts of the study area in the initial ablation
753 and ablation periods. However, the influence of evaporation on isotope and d-excess
754 is prevalent in most places except the southeastern part of the study area. Meanwhile,
755 this results also indicated that there may be a hysteresis for the influence of
756 meteorological factors on isotopes and d-excess. The altitude effect is only present
757 during the ablation periods in 2016 and 2018, and the altitude effect was −0.16‰/100
758 m ($p < 0.05$) and −0.14‰/100 m ($p < 0.05$). The slope of LEL for river water showed
759 an increasing trend from initial ablation to end ablation in 2016. Meanwhile, the
760 intercept of LEL for river water also increased from the initial ablation to the end
761 ablation period. Moreover, the mixed segmentation model of the end-member is used
762 to determine the contribution proportion of different water sources to the target water.
763 The results showed that the supra-permafrost water was the major recharge source for
764 the permafrost area river in the study area. Meanwhile, the glacier and snow
765 meltwater contributed little to the permafrost area river in the initial and end ablation
766 periods. For the mainstream, the proportion was 35.93% in initial and end ablation
767 periods, and 45.55% in the ablation period. However, the proportion was 47.49% in
768 the initial and end ablation periods, and 36.47% in the ablation period.
769 Theproportion of glacier and snow meltwater for the mainstream (16.59%) was higher
770 than that for the permafrost area river (3.25%) but was lower than that for the glacier
771 permafrost area river (19.44%) in the initial and end ablation periods. Meanwhile, the
772 proportion of glacier and snow meltwater for the mainstream (17.98%) was higher

than that for the permafrost area river (13.95%) but was lower than that for the glacier permafrost area river (27.30%) in the ablation period.

Acknowledges

This study was supported by National "Plan of Ten Thousand People" Youth Top Talent Project, the Second Tibetan Plateau Scientific Expedition and Research Program(STEP), Grant No. 2019QZKK0405, the Youth Innovation Promotion Association, CAS (2013274), Open funding from the Key Laboratory of Mountain Hazards and Earth Surface Process the open funding from State Key Laboratory of Loess and Quaternary Geology (SKLLQG1814).

References

Abongwa, P. T., & Atekwana, E. A. : A laboratory study investigating the effects of dilution by precipitation on dissolved inorganic carbon and stable isotope evolution in surface waters. Environ Sci Pollu Res, 25(20), 19941-19952. https://doi.org/10.1007/s11356-018-2085-0, 2018.

Banner, J. L., & Hanson, G. N. : Calculation of simultaneous isotopic and trace element variations during water-rock interaction with applications to carbonate diagenesis. Geochim Cosmochim Ac, 54(11), 3123-3137. https://doi.org/10.1016/0016-7037(90)90128-8, 1990.

Boucher, J. L., & Carey, S. K.: Exploring runoff processes using chemical, isotopic

796 and hydrometric data in a discontinuous permafrost catchment. Hydro Res, 41(6),
797 508-519. https://doi.org/10.2166/nh.2010.146, 2010.
798 Chang, J., Wang, G., & Mao, T. : Simulation and prediction of suprapermafrost
799 groundwater level variation in response to climate change using a neural network
800 model. J Hydro, 529, 1211-1220. https://doi.org/10.1016/j.jhydrol.2015.09.038,
801 2015.
802 Fan, Y., Chen, Y., Li, X., Li, W., & Li, Q. : Characteristics of water isotopes and
803 ice-snowmelt quantification in the Tizinafu River, north Kunlun Mountains,
804 Central Asia. Quater inter, 380, 116-122.
805 https://doi.org/10.1016/j.quaint.2014.05.020, 2015.
806 Halder, J., Terzer, S., Wassenaar, L. I., Araguás-Araguás, L. J., & Aggarwal, P. K. :
807 The Global Network of Isotopes in Rivers (GNIR): integration of water isotopes
808 in watershed observation and riverine research. Hydrol Earth Sys Sc, 19(8),
809 3419-3431. https://doi.org/10.5194/hess-19-3419-2015, 2015.
810 Hooper, R. P. : Diagnostic tools for mixing models of stream water chemistry. Water
811 Resour Res, 39(3): 1055. https://doi.org/10.1029/2002WR001528, 2003.
812 Horita, J., Driesner, T., & Cole, D. R. : Hydrogen isotope fractionation in the system
813 brucite-water±NaCl to elevated temperatures and pressures: Implications for the
814 isotopic property of NaCl fluids under geologic conditions. Geochim
815 Cosmochim Aca, 235, 140-152. https://doi.org/10.1016/j.gca.2018.05.031, 2018.
816 Gao, H., He, X., Ye, B., & Pu, J. : Modeling the runoff and glacier mass balance in a
817 small watershed on the Central Tibetan Plateau, China, from 1955 to 2008.

Hydro Pro, 26(11), 1593-1603. https://doi.org/10.1002/hyp.8256, 2012.

Genereux, D. : Quantifying uncertainty in tracer‐based hydrograph separations. Water Resour Res, 34(4), 915-919. https://doi.org/10.1029/98WR00010, 1998.

Gu, W. Z., & Longinelli, A. : A case study on the hydrological significance of stable isotope data on alpine catchments with snow cover and glaciers, Xinjiang, China. IAHS Publications-Publications of the Inter Asso Hydro Sci, 218, 371-384, 1993.

Jin, H., Zhao, L., Wang, S., & Jin, R. : Thermal regimes and degradation modes of permafrost along the Qinghai-Tibet Highway. Sci China Ser D: Earth Sci, 49(11), 1170-1183. https://doi.org/10.1007/s11430-006-2003-z, 2006.

Kang, S., Zhang, Y., Qin, D., Ren, J., Zhang, Q., Grigholm, B., & Mayewski, P. A. : Recent temperature increase recorded in an ice core in the source region of Yangtze River. Chinese Sci Bull, 52(6), 825-831. https://doi.org/10.1007/s11434-007-0140-1, 2007.

Klaus, J., & McDonnell, J. J. : Hydrograph separation using stable isotopes: Review and evaluation. J Hydro, 505, 47-64. https://doi.org/10.1016/j.jhydrol.2013.09.006, 2013.

Kong, Y., & Pang, Z. : Evaluating the sensitivity of glacier rivers to climate change based on hydrograph separation of discharge. J Hydro, 434, 121-129. https://doi.org/10.1016/j.jhydrol.2012.02.029, 2012.

Lafrenière, M. J., & Lamoureux, S. F. : Effects of changing permafrost conditions on hydrological processes and fluvial fluxes. Earth-Sci Rev, 191,212-223.

https://doi.org/10.1016/j.earscirev.2019.02.018, 2019.

Li, C., Yang, S., Lian, E., Yang, C., Deng, K., & Liu, Z. : Damming effect on the Changjiang (Yangtze River) river water cycle based on stable hydrogen and oxygen isotopic records. J Geochem Explor, 165, 125-133. https://doi.org/10.1016/j.gexplo.2016.03.006, 2016.

Li, Z.X., Qi, F., Wei, L., Tingting, W., Aifang, C., Yan, G., ... & Bing, J. : Study on the contribution of cryosphere to runoff in the cold alpine basin: A case study of Hulugou River Basin in the Qilian Mountains. Global Planet Change, 122, 345-361. https://doi.org/10.1016/j.gloplacha.2014.10.001, 2014a.

Li, Z.X., Qi, F., Wei, L., Tingting, W., Yan, G., Yamin, W., ... & Li, L. : Spatial and temporal trend of potential evapotranspiration and related driving forces in Southwestern China, during 1961–2009. Quater inter, 336, 127-144. https://doi.org/10.1016/j.quaint.2013.12.045, 2014b.

Li, Z.X., Qi, F., Wang, Q. J., Song, Y., Aifang, C., & Jianguo, L. : Contribution from frozen soil meltwater to runoff in an in-land river basin under water scarcity by isotopic tracing in northwestern China. Global Planet Change, 136, 41-51. https://doi.org/10.1016/j.gloplacha.2015.12.002, 2016a.

Li, Z.X., Qi, F., Zongjie, L., Ruifeng, Y., Juan, G., & Yuemin, L. : Climate background, fact and hydrological effect of multiphase water transformation in cold regions of the Western China: A review. Earth-Sci Re, 190,33-57. https://doi.org/10.1016/j.earscirev.2018.12.004, 2018.

Li, Z.X., Qi, F., Wang, Q. J., Song, Y., Jianguo, L., Yongge, L., & Yamin, W. :

862 Quantitative evaluation on the influence from cryosphere meltwater on runoff in
863 an inland river basin of China. Global Planet Change, 143, 189-195.
864 https://doi.org/10.1016/j.gloplacha.2016.06.005, 2016b.
865 Li, Z.X., Qi, F., Wei, L., Tingting, W., Xiaoyan, G., Zongjie, L., ... & Yaoxaun, S. :
866 The stable isotope evolution in Shiyi glacier system during the ablation period in
867 the north of Tibetan Plateau, China. Quater inter, 380, 262-271.
868 https://doi.org/10.1016/j.quaint.2015.02.013, 2015.
869 Li, Z., Yuan, R., Feng, Q., Zhang, B., Lv, Y., Li, Y., ... & Shi, Y. : Climate background,
870 relative rate, and runoff effect of multiphase water transformation in Qilian
871 Mountains, the third pole region. Sci Total Environ, 663, 315-328.
872 https://doi.org/10.1016/j.scitotenv.2019.01.339, 2019.
873 Li, Z.J., Song, L. L., Jing-zhu, M., & Li, Y. G. : The characteristics changes of pH and
874 EC of atmospheric precipitation and analysis on the source of acid rain in the
875 source area of the Yangtze River from 2010 to 2015. Atmos environ, 156, 61-69.
876 https://doi.org/10.1016/j.atmosenv.2017.02.025, 2017.
877 Li, Z.J., Zong-Xing, L., Ling-Ling, S., Jin-Zhu, M., & Yong, S. : Environment
878 significance and hydrochemical characteristics of supra-permafrost water in the
879 source region of the Yangtze River. Sci total environ, 644, 1141-1151.
880 https://doi.org/10.1016/j.scitotenv.2018.07.029, 2018.
881 Liang, E., Shao, X., & Qin, N. : Tree-ring based summer temperature reconstruction
882 for the source region of the Yangtze River on the Tibetan Plateau. Global Planet
883 Change, 61(3-4), 313-320. https://doi.org/10.1016/j.gloplacha.2007.10.008,

884 2008.

885 Liu, F., Williams, M. W., & Caine, N. : Source waters and flow paths in an alpine
886 catchment, Colorado Front Range, United States. Water Resour Res, 40(9), 1-17.
887 https://doi.org/10.1029/2004WR003076, 2004.

888 Lutz, A. F., Immerzeel, W. W., Shrestha, A. B., & Bierkens, M. F. P. : Consistent
889 increase in High Asia's runoff due to increasing glacier melt and precipitation.
890 Nat Clim Change, 4(7), 587. https://doi.org/10.1038/nclimate2237, 2014.

891 Maurya, A. S., Shah, M., Deshpande, R. D., Bhardwaj, R. M., Prasad, A., & Gupta, S.
892 K. : Hydrograph separation and precipitation source identification using stable
893 water isotopes and conductivity: River Ganga at Himalayan foothills. Hydro Pro,
894 25(10), 1521-1530. https://doi.org/10.1002/hyp.7912, 2011.

895 McGuire, A. D., Wirth, C., Apps, M., Beringer, J., Clein, J., Epstein, H., ... & Efremov,
896 D. : Environmental variation, vegetation distribution, carbon dynamics and
897 water/energy exchange at high latitudes. J Veget Sci, 13(3), 301-314.
898 https://doi.org/10.1111/j.1654-1103.2002.tb02055.x, 2002.

899 Mu, Y., Ma, W., Li, G., Niu, F., Liu, Y., & Mao, Y. : Impacts of supra-permafrost
900 water ponding and drainage on a railway embankment in continuous permafrost
901 zone, the interior of the Qinghai-Tibet Plateau. Cold Reg Sci Tech, 154, 23-31.
902 https://doi.org/10.1016/j.coldregions.2018.06.007, 2018.

903 Orlowski, N., Breuer, L., & McDonnell, J. J. : Critical issues with cryogenic
904 extraction of soil water for stable isotope analysis. Ecohydro, 9(1), 1-5.
905 https://doi.org/10.1002/eco.1722, 2016.

906 Pan, X., Yu, Q., You, Y., Chun, K. P., Shi, X., & Li, Y. : Contribution of
907 supra-permafrost discharge to thermokarst lake water balances on the
908 northeastern Qinghai-Tibet Plateau. J Hydro, 555, 621-630.
909 https://doi.org/10.1016/j.jhydrol.2017.10.046, 2017.
910 Peng, T. R., Wang, C. H., Huang, C. C., Fei, L. Y., Chen, C. T. A., & Hwong, J. L. :
911 Stable isotopic characteristic of Taiwan's precipitation: A case study of western
912 Pacific monsoon region. Earth Planet Sci Let, 289(3-4), 357-366.
913 https://doi.org/10.1016/j.epsl.2009.11.024, 2010.
914 Prasch, M., Mauser, W., & Weber, M. : Quantifying present and future glacier
915 melt-water contribution to runoff in a central Himalayan river basin. Cryos, 7(3).
916 https://doi:10.5194/tc-7-889-2013, 2013.
917 Pu, T., He, Y., Zhu, G., Zhang, N., Du, J., & Wang, C. : Characteristics of water stable
918 isotopes and hydrograph separation in Baishui catchment during the wet season
919 in Mt. Yulong region, south western China. Hydro Pro, 27(25), 3641-3648.
920 https://doi.org/10.1002/hyp.9479, 2013.
921 Pu, J. : Glacier Inventory of China: The Yangtze River Drainage Basin. Lanzhou:
922 Gansu Culture Press, 1-81, 1994.
923 Qu, J. H., Lu, S. B., Gao, Z. P., Li, W., Li, Z., & Yu, F. : Research on
924 hydrogeochemical characteristics and transformation relationships between surface
925 water and groundwater in the Weihe River. Hydrol Earth sys sc,1-14.
926 https://doi.org/10.5194/hess-2017-654, 2017.
927 Shi, Y., Niu, F., Lin, Z., & Luo, J. : Freezing/thawing index variations over the
928 circum-Arctic from 1901 to 2015 and the permafrost extent. Sci Total Environ,

660, 1294-1305. https://doi.org/10.1016/j.scitotenv.2019.01.121, 2019.

Uhlenbrook, S., & Hoeg, S. : Quantifying uncertainties in tracer - based hydrograph separations: a case study for two - , three - and five - component hydrograph separations in a mountainous catchment. Hydro Pro, 17(2), 431-453. https://doi.org/10.1002/hyp.1134, 2003.

Walker, D. A., Jia, G. J., Epstein, H. E., Raynolds, M. K., Chapin Iii, F. S., Copass, C., ... & Nelson, F. : Vegetation - soil - thaw - depth relationships along a low - arctic bioclimate gradient, Alaska: Synthesis of information from the ATLAS studies. Perma Peri Pro, 14(2), 103-123. https://doi.org/10.1002/ppp.452, 2003.

Wang, G., Liu, G., & Liu, L. A. : Spatial scale effect on seasonal streamflows in permafrost catchments on the Qinghai–Tibet Plateau. Hydro Pro, 26(7), 973-984. https://doi.org/10.1002/hyp.8187, 2012.

Wang, G., Hu, H., & Li, T. : The influence of freeze–thaw cycles of active soil layer on surface runoff in a permafrost watershed. J Hydro, 375(3-4), 438-449. https://doi.org/10.1016/j.jhydrol.2009.06.046, 2009.

Wang, G., Tianxu, M., Juan, C., Chunlin, S., & Kewei, H. : Processes of runoff generation operating during the spring and autumn seasons in a permafrost catchment on semi-arid plateaus. J hydro, 550, 307-317. https://doi.org/10.1016/j.jhydrol.2017.05.020, 2017.

Wang, G., Yuanshou, L., Yibo, W., & Qingbo, W. : Effects of permafrost thawing on vegetation and soil carbon pool losses on the Qinghai–Tibet Plateau, China.

951 Geoderma, 143(1-2), 143-152. https://doi.org/10.1016/j.geoderma.2007.10.023,
952 2008.
953 Wang, T., Wu, T., Wang, P., Li, R., Xie, C., & Zou, D. : Spatial distribution and
954 changes of permafrost on the Qinghai-Tibet Plateau revealed by statistical
955 models during the period of 1980 to 2010. Sci Total Environ, 650, 661-670.
956 https://doi.org/10.1016/j.scitotenv.2018.08.398, 2019.
957 Wang, X., Chen, R., Liu, G., Yang, Y., Song, Y., Liu, J., ... & Wang, L. : Spatial
958 distributions and temporal variations of the near-surface soil freeze state across
959 China under climate change. Global planet change, 172, 150-158.
960 https://doi.org/10.1016/j.gloplacha.2018.09.016, 2019.
961 West, A. G., February, E. C., & Bowen, G. J. : Spatial analysis of hydrogen and
962 oxygen stable isotopes ("isoscapes") in ground water and tap water across South
963 Africa. J Geochem Explo, 145, 213-222.
964 https://doi.org/10.1016/j.gexplo.2014.06.009, 2014.
965 Wu, Q., Hou, Y., Yun, H., & Liu, Y. : Changes in active-layer thickness and
966 near-surface permafrost between 2002 and 2012 in alpine ecosystems,
967 Qinghai–Xizang (Tibet) Plateau, China. Global Planet Change, 124, 149-155.
968 https://doi.org/10.1016/j.gloplacha.2014.09.002, 2015.
969 Yang, L., Song, X., Zhang, Y., Han, D., Zhang, B., & Long, D. : Characterizing
970 interactions between surface water and groundwater in the Jialu River basin
971 using major ion chemistry and stable isotopes. Hydrol Earth Sys Sc, 16(11),
972 4265-4277. https://doi.org/10.5194/hess-16-4265-2012, 2012.

973 Yang, M., Nelson, F. E., Shiklomanov, N. I., Guo, D., & Wan, G. : Permafrost
974 degradation and its environmental effects on the Tibetan Plateau: A review of
975 recent research. Earth-Sci Re, 103(1-2), 31-44.
976 https://doi.org/10.1016/j.earscirev.2010.07.002, 2010.
977 Yang, Q., Mu, H., Wang, H., Ye, X., Ma, H., & Martín, J. D. : Quantitative evaluation
978 of groundwater recharge and evaporation intensity with stable oxygen and
979 hydrogen isotopes in a semi‐arid region, Northwest China. Hydro pro, 32(9),
980 1130-1136. https://doi.org/10.1002/hyp.11474, 2018.
981 Yao, Z., Liu, Z., Huang, H., Liu, G., & Wu, S. : Statistical estimation of the impacts of
982 glaciers and climate change on river runoff in the headwaters of the Yangtze
983 River. Quater inter, 336, 89-97. https://doi.org/10.1016/j.quaint.2013.04.026,
984 2014.
985 Yu, G. A., Liu, L., Li, Z., Li, Y., Huang, H., Brierley, G., ... & Pan, B. : Fluvial
986 diversity in relation to valley setting in the source region of the Yangtze and
987 Yellow Rivers. J Geog Sci, 23(5), 817-832.
988 https://doi.org/10.1007/s11442-013-1046-2, 2013.
989 Yu, G. A., Brierley, G., Huang, H. Q., Wang, Z., Blue, B., & Ma, Y. : An
990 environmental gradient of vegetative controls upon channel planform in the
991 source region of the Yangtze and Yellow Rivers. Catena, 119, 143-153.
992 https://doi.org/10.1016/j.catena.2014.02.010, 2014.
993 Zhang, Y., Ohata, T., & Kadota, T. : Land-surface hydrological processes in the
994 permafrost region of the eastern Tibetan Plateau. J Hydro, 283(1-4), 41-56.

https://doi.org/10.1016/S0022-1694(03)00240-3, 2003.

Zhao, L., Ping, C. L., Yang, D., Cheng, G., Ding, Y., & Liu, S. : Changes of climate and seasonally frozen ground over the past 30 years in Qinghai–Xizang (Tibetan) Plateau, China. Global Planet Change, 43(1-2), 19-31. https://doi.org/10.1016/j.gloplacha.2004.02.003, 2004.

Zhu, X., Wu, T., Zhao, L., Yang, C., Zhang, H., Xie, C., ... & Du, Y. : Exploring the contribution of precipitation to water within the active layer during the thawing period in the permafrost regions of central Qinghai-Tibet Plateau by stable isotopic tracing. Sci Total Environ, 661, 630-644. https://doi.org/10.1016/j.scitotenv.2019.01.064, 2019.

Tables:

Table 1 The correlation analysis of $\delta^{18}O$ and d-excess and meteorological factors in the fixed point (TTH and ZMD) from March,16 to July, 18.

Table 1 The correlation analysis of $\delta^{18}O$ and d-excess and meteorological factors in the fixed point (TTH and ZMD) from March,16 to July, 18.

	Precipitation (mm)	Temperature (℃)	Ralative humidity (%)	Evaporation (mm)	$\delta^{18}O$(‰)	D-excess (‰)
Precipitation(mm)	1					
Temperature(℃)	0.853**	1				
Ralative humidity(%)	0.760**	0.836**	1			
Evaporation(mm)	0.658**	0.865**	0.586**	1		
$\delta^{18}O$(‰)	-0.518**	-0.671**	-0.555**	-0.636**	1	
D-excess(‰)	0.500**	0.602**	0.524**	0.533**	-0.568**	1

Note: **, Correlation is significant at the 0.01 level (2-tailed).

Figures:

Fig.1 The map of the study area and the sampling point of river water in different ablation period

(Fig.1a was the detail location of the study area in China and Asian and the distribution of fixed point for precipitation, river water and glacier and snow meltwater; Fig.1b was the distribution of sampling point in initial ablation in 2016; Fig.1c was the distribution of sampling point in ablation in 2016; Fig.1d was the distribution of sampling point in end ablation in 2016; Fig.1e was the distribution of sampling point in ablation in 2017; Fig.1f was the distribution of sampling point in ablation in 2018)

Fig.2 Temporal variation of $\delta^{18}O$ and d-excess during the sampling period in study area

(This figure mainly showed the temporal variation of $\delta^{18}O$ and d-excess for different type runoff based on different ablation in 2016 and strong ablation from 2016 to 2018; Fig.2a, b, c showed the change of $\delta^{18}O$ and d-excess in different ablation period for mainstream, glacier and snow runoff and river in permafrost area; Fig.2d, e, f showed the change of $\delta^{18}O$ and d-excess in ablation period from 2016 to 2018 for mainstream, glacier and snow runoff and river in permafrost area)

Fig.3 Spatial variation of $\delta^{18}O$ based on different ablation in 2016 and ablation from 2016 to 2018

Fig.4 Spatial variation of d-excess based on different ablation in 2016 and ablation from 2016 to 2018

Fig.5 The variation of $\delta^{18}O$ and d-excess with the altitude change in study area

(Fig.5a was the variation of $\delta^{18}O$ and d-excess with the altitude change for mainstream; Fig.5b

1103 was the variation of $\delta^{18}O$ and d-excess with the altitude change for river in glacier permafrost
1104 area;Fig.5c was the variation of $\delta^{18}O$ and d-excess with the altitude change for river in permafrost
1105 area; IA in 2016 represents Initial ablation in 2016; A in 2016 represents Ablation in 2016; EA in
1106 2016 represents End ablation in 2016; A in 2017 represents Ablation in 2017; A in 2018
1107 represents Ablation in 2018)

1108 Fig.6 The variation of location evaporation line (LEL) of river water based on
1109 different ablation in 2016 and ablation from 2016 to 2018

1110 Fig.7 The distribution of δD and $\delta^{18}O$ for river water among other water bodies in
1111 study area

1112 (Fig.7a was the plot of $\delta^{18}O$ for river water in different type, supra-permafrost water, glacier snow
1113 meltwater and precipitation; Fig.7b was the plot of δD for river water in different type,
1114 supra-permafrost water, glacier snow meltwater and precipitation; Fig.7c was the plot of δD
1115 versus $\delta^{18}O$ for river water, supra-permafrost water, glacier snow meltwater and precipitation)

1116 Fig.8 Three end element diagram using the mean values of $\delta^{18}O$ and d-excess for river
1117 water in different ablation in 2016 and ablation from 2016 to 2018

1118 Fig.9 Recharge proportion from possible sources to river water in different altitude
1119 during different ablation in 2016 and ablation from 2016 to 2018

1120 Fig.10 Variation of meteorological factors during sampling period

1121 (Shadow represents the ablation period)

1122 Fig.11 Conceptual model map of the recharge form and proportion of the river water
1123 in different ablation period

1124 (Dark green represents the basin of river in permafrost area; Gray and light green represents the

basin of the river in glacier permafrost area)

1167 Fig.1

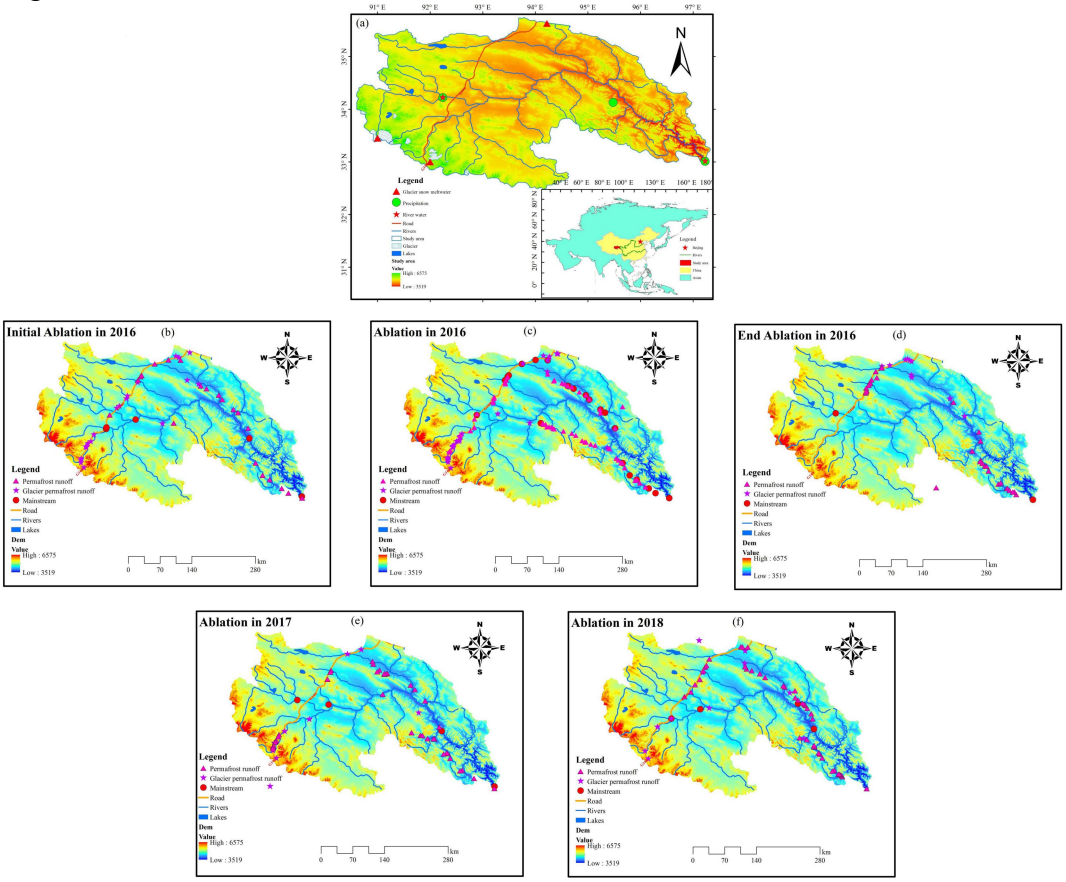

1168

1169 Fig.1 The map of the study area and the sampling point of river water in different

1170 ablation period (Fig.1a was the detail location of the study area in China and Asian and the

1171 distribution of fixed point for precipitation, river water and glacier and snow meltwater; Fig.1b

1172 was the distribution of sampling point in initial ablation in 2016; Fig.1c was the distribution of

1173 sampling point in ablation in 2016; Fig.1d was the distribution of sampling point in end ablation in

1174 2016; Fig.1e was the distribution of sampling point in ablation in 2017; Fig.1f was the distribution

1175 of sampling point in ablation in 2018)

1176
1177
1178
1179
1180
1181
1182
1183

Fig.2

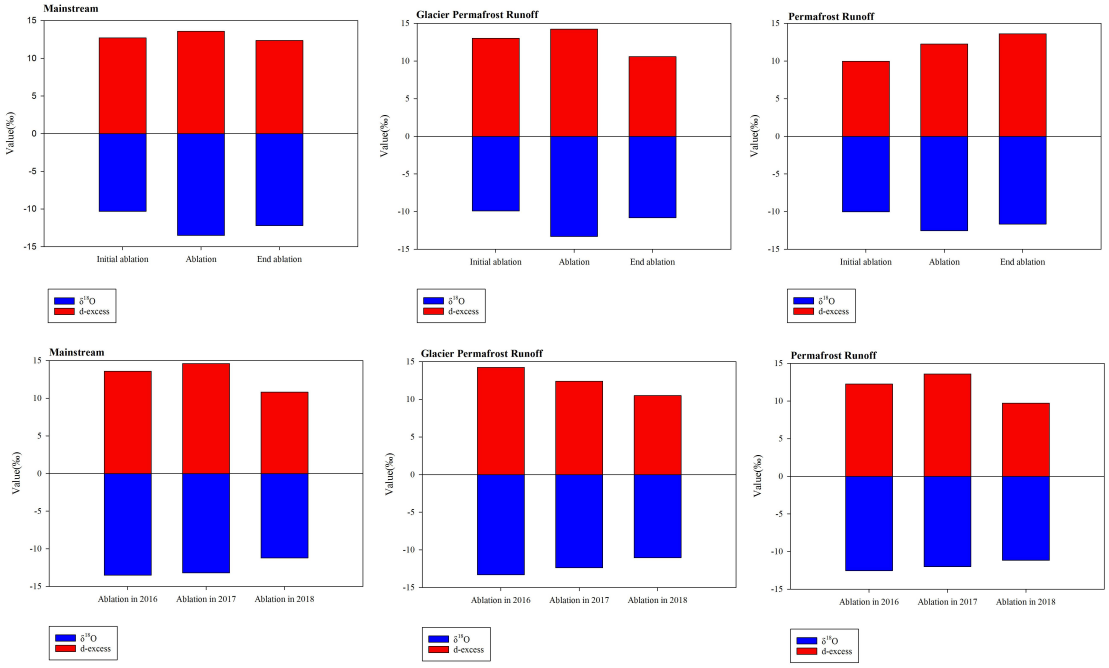

Fig.2 Temporal variation of $\delta^{18}O$ and d-excess during the sampling period in study area (This figure mainly showed the temporal variation of $\delta^{18}O$ and d-excess for different type runoff based on different ablation in 2016 and strong ablation from 2016 to 2018; Fig.2a, b, c showed the change of $\delta^{18}O$ and d-excess in different ablation period for mainstream, glacier and snow runoff and river in permafrost area; Fig.2d, e, f showed the change of $\delta^{18}O$ and d-excess in ablation period from 2016 to 2018 for mainstream, glacier and snow runoff and river in permafrost area)

Fig.3

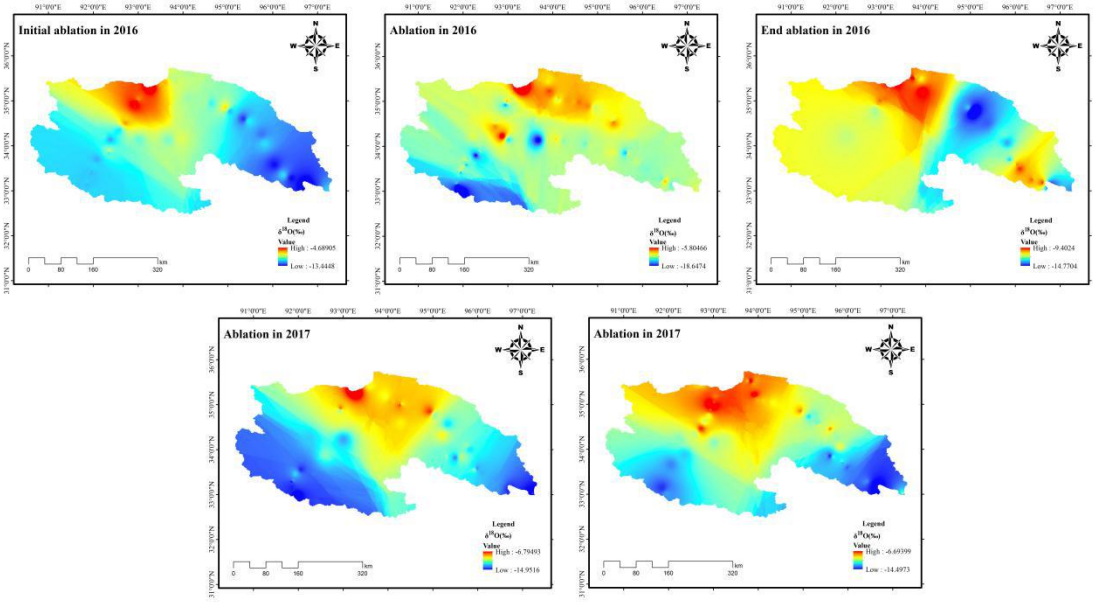

Fig.3 Spatial variation of $\delta^{18}O$ based on different ablation in 2016 and ablation from 2016 to 2018

Fig.4

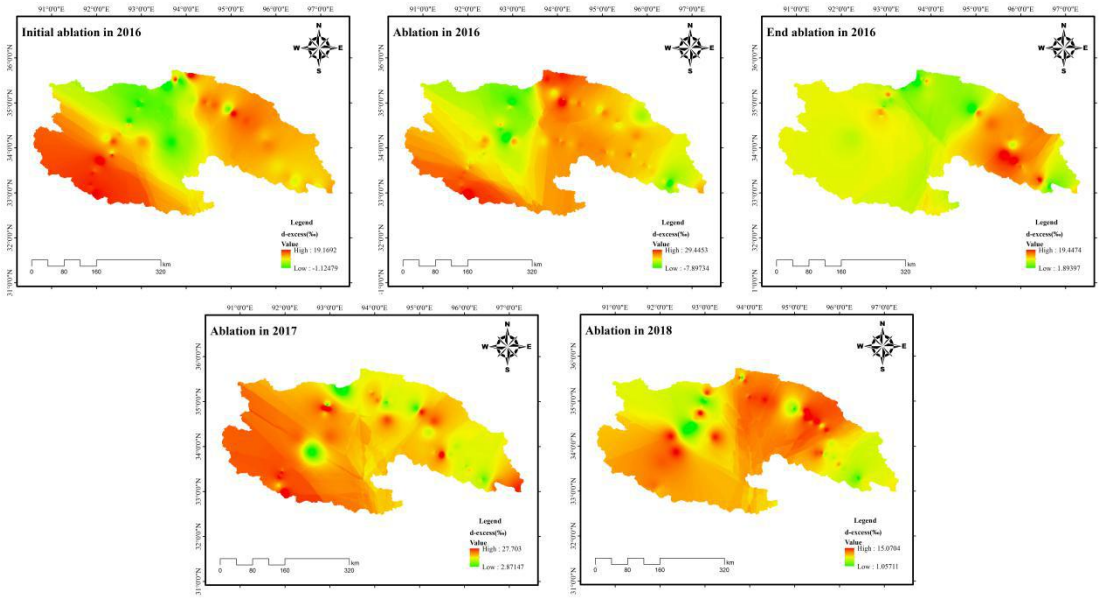

Fig.4 Spatial variation of d-excess based on different ablation in 2016 and ablation from 2016 to 2018

Fig.5

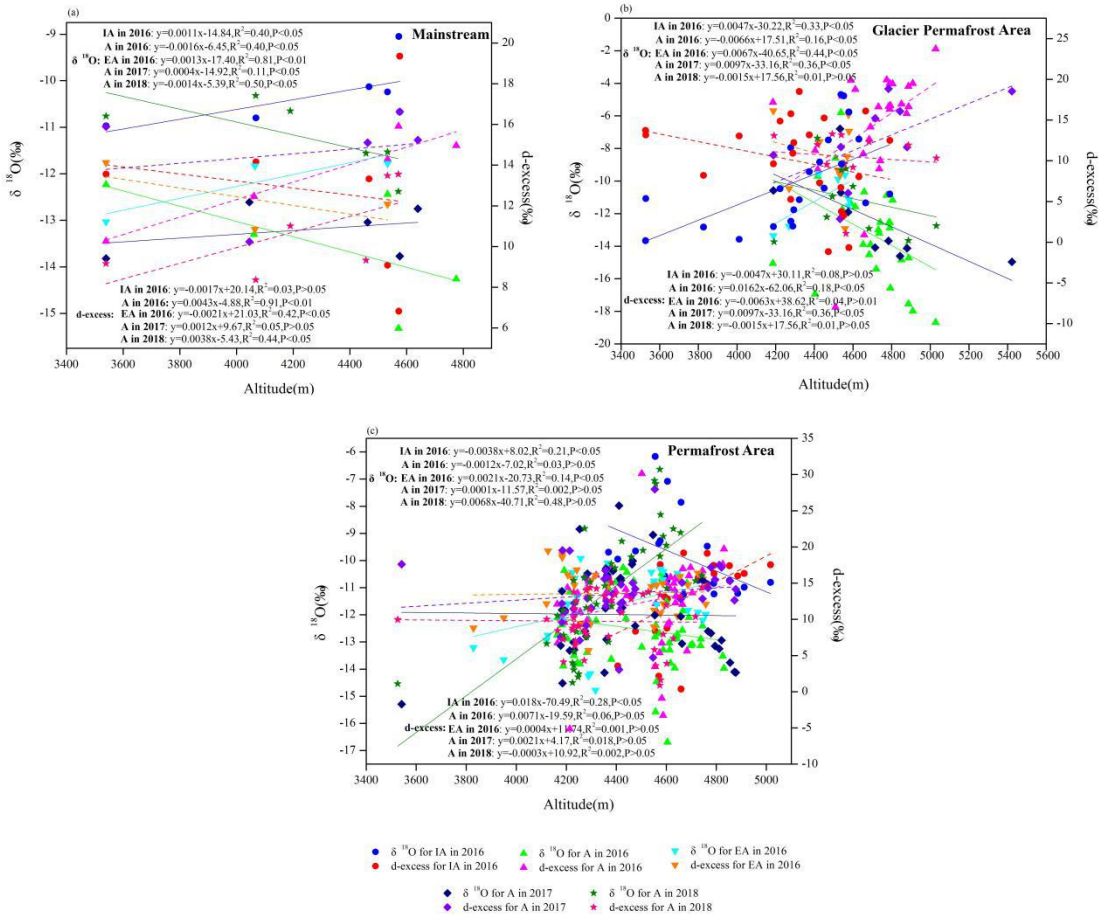

Fig.5 The variation of $\delta^{18}O$ and d-excess with the altitude change in study area (Fig.5a was the variation of $\delta^{18}O$ and d-excess with the altitude change for mainstream; Fig.5b was the variation of $\delta^{18}O$ and d-excess with the altitude change for river in glacier permafrost area;Fig.5c was the variation of $\delta^{18}O$ and d-excess with the altitude change for river in permafrost area; IA in 2016 represents Initial ablation in 2016; A in 2016 represents Ablation in 2016; EA in 2016 represents End ablation in 2016; A in 2017 represents Ablation in 2017; A in 2018 represents Ablation in 2018)

Fig.6

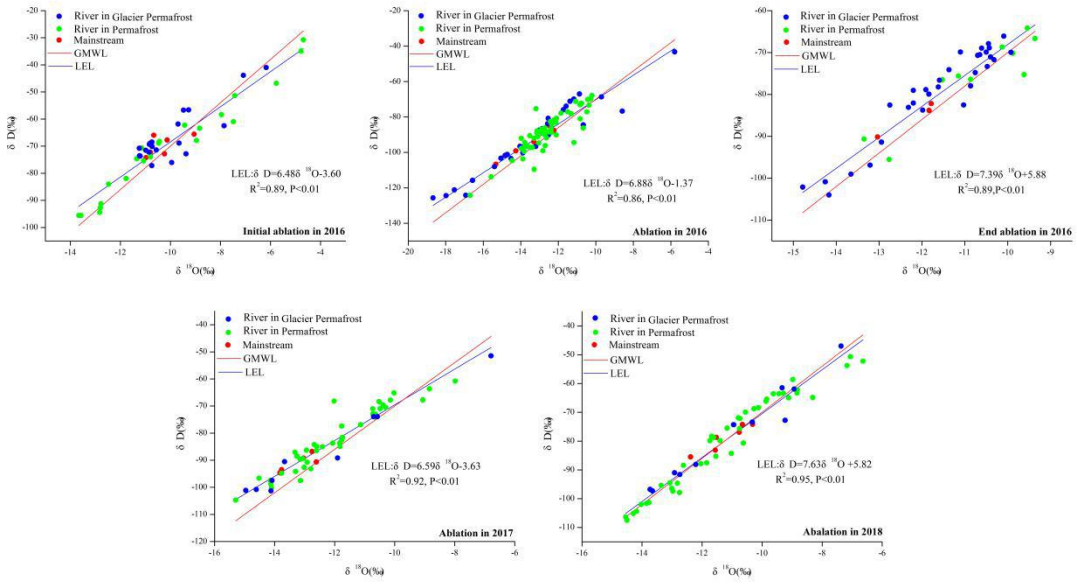

Fig.6 The variation of location evaporation line (LEL) of river water based on different ablation in 2016 and ablation from 2016 to 2018

Fig.7

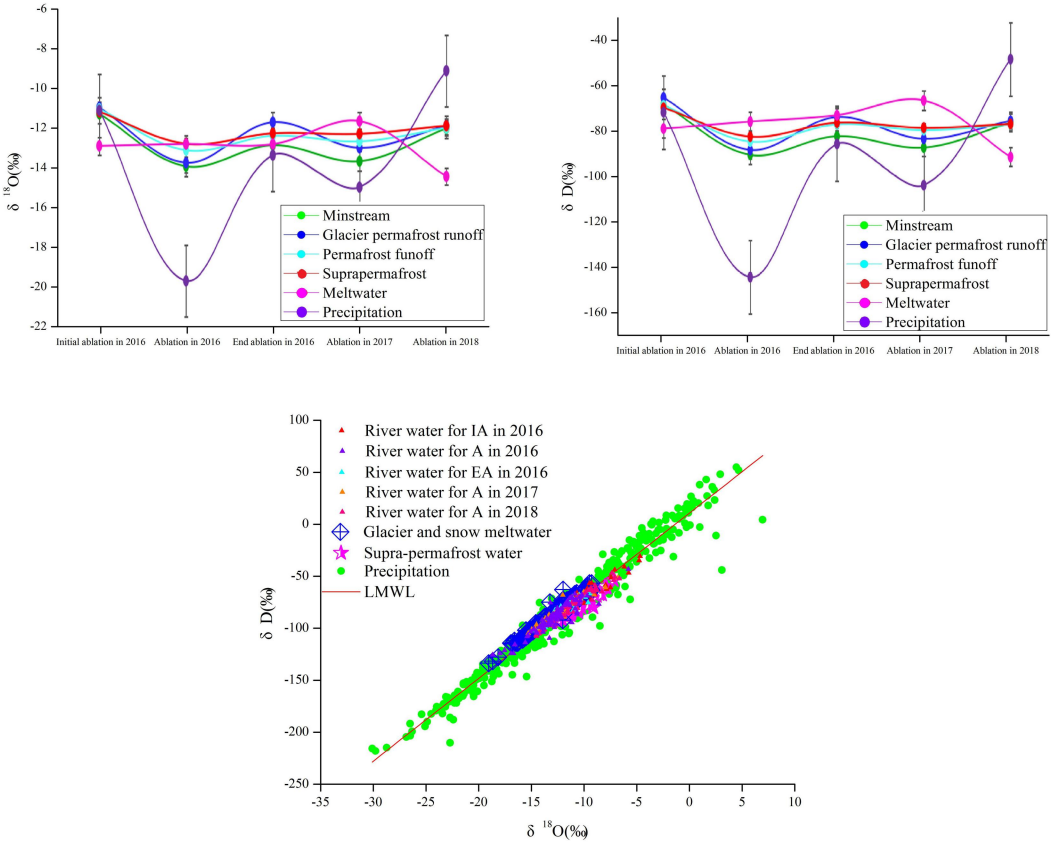

Fig.7 The distribution of δD and $\delta^{18}O$ for river water among other water bodies in study area (Fig.7a was the plot of $\delta^{18}O$ for river water in different type, supra-permafrost water, glacier snow meltwater and precipitation; Fig.7b was the plot of δD for river water in different type, supra-permafrost water, glacier snow meltwater and precipitation; Fig.7c was the plot of δD versus $\delta^{18}O$ for river water, supra-permafrost water, glacier snow meltwater and precipitation)

Fig.8

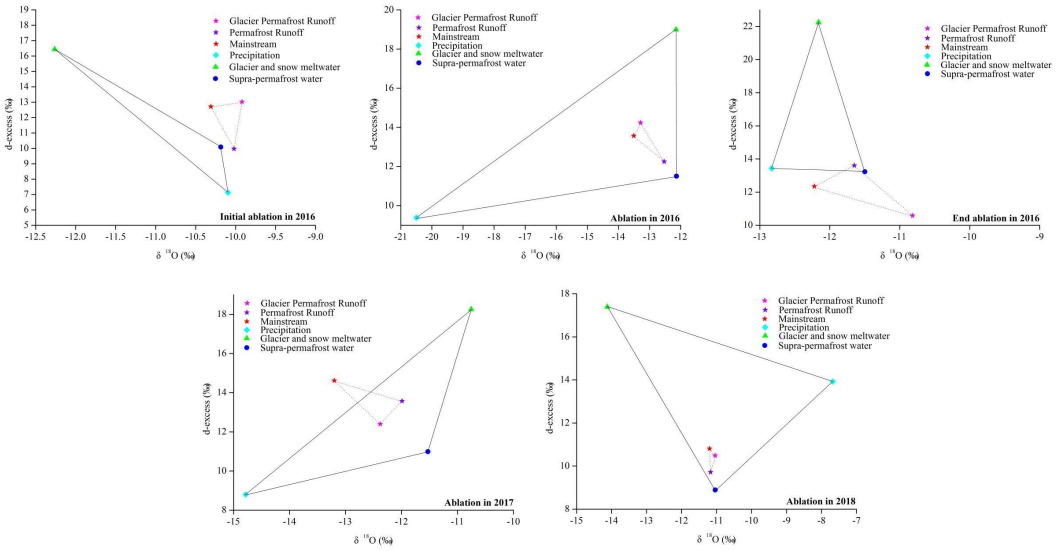

Fig.8 Three end element diagram using the mean values of $\delta^{18}O$ and d-excess for river water in different ablation in 2016 and ablation from 2016 to 2018

Fig.9

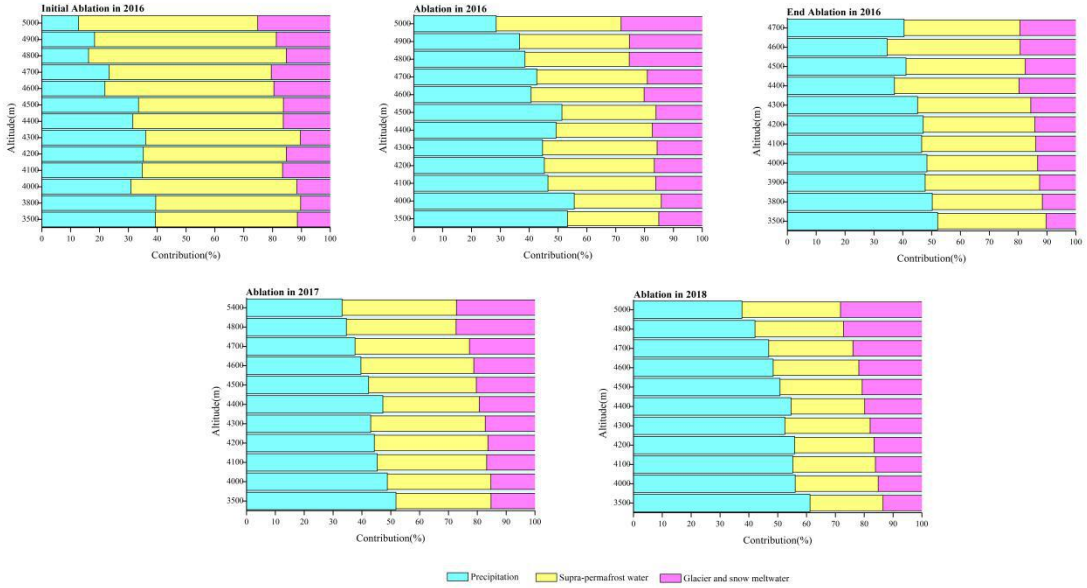

Fig.9 Recharge proportion from possible sources to river water in different altitude during different ablation in 2016 and ablation from 2016 to 2018

Fig.10

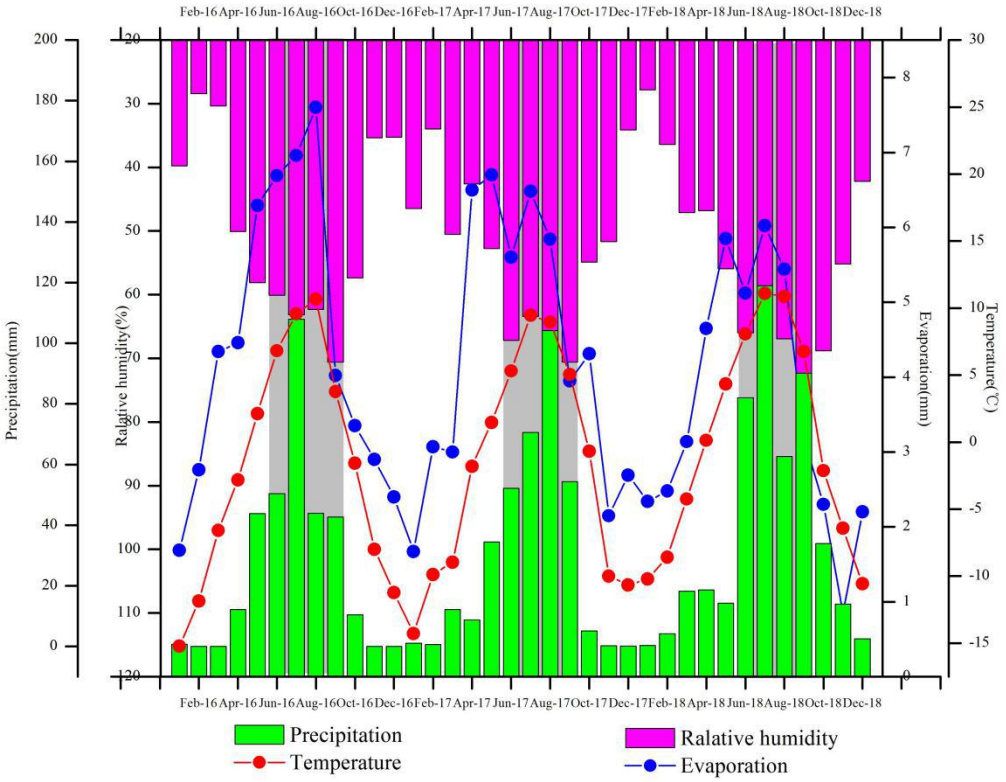

Fig.10 Variation of meteorological factors during sampling period (Shadow represents the ablation period)

Fig.11

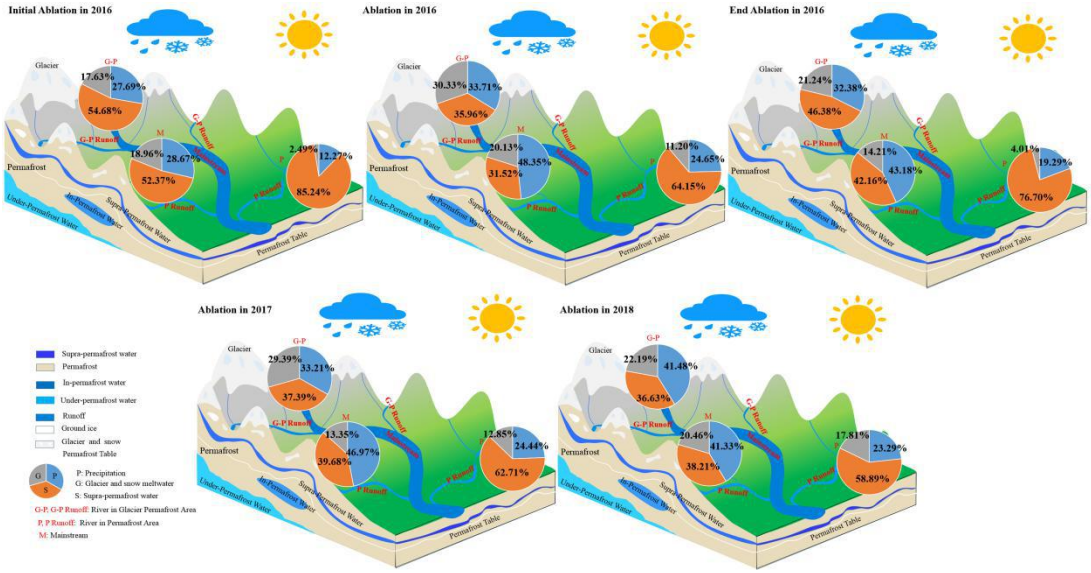

Fig.11 Conceptual model map of the recharge form and proportion of the river water in different ablation period (Dark green represents the basin of river in permafrost area; Gray and light green represents the basin of the river in glacier permafrost area)